Research papers

Critical diameter for a single-tank molten salt storage – Parametric study on structural tank design

Freerk Klasing [a],[*], Mark Schmitz [b], Christian Gerdes [c], Christian Odenthal [a], Thomas Bauer [a]

[a] *German Aerospace Center, 51147 Cologne, Germany*
[b] *TSKFlagsol Engineering GmbH, 50678 Cologne, Germany*
[c] *JPM Ingenieurtechnik GmbH, 24558 Henstedt-Ulzburg, Germany*

A R T I C L E   I N F O

A B S T R A C T

Molten salt thermal energy storage (TES) is a cost-effective option for grid-connected storage in both concentrating solar power (CSP) plants and retrofitted thermal power plants in a multimegawatt scale. Current systems use two tanks (hot and cold), but future systems may use a single tank with a transient temperature profile (hot in the top and cold in the bottom) to reduce costs and space. However, the structural and mechanical design of large-scale molten salt single-tank storages at 560 °C has not been fully explored, and the impact of increasing the operating temperature to 620 °C is still uncertain. The challenge presented by a single tank is the existence of a temperature profile that results in a varying thermal expansion of the tank shell along its height. In the case of larger tanks, this discrepancy can reach a magnitude of centimeters, which in turn gives rise to bending moments. To the best of our knowledge, this study addresses the issue of bending stresses in large-sized high-temperature tanks with thermal stratification for the first time. The modelling approach is applied to single-tank CSP TES systems as a case study to evaluate the constraints imposed by tank size and wall thickness.

With the help of experimentally validated numerical methods, it is revealed that a low thermocline thickness can be a limiting factor for large tank diameters. It is shown that the temperature has a major influence on maximum possible tank size: if the operating temperature is raised from 560 °C to 620 °C, the permitted tank diameter is significantly reduced when using the same tank wall material. A possible approach is to use a more heat resistant steel for 620 °C. Results of the parametric study show that designing a single tank below a critical diameter only requires a moderate increase of the wall thickness compared to the two-tank system with constant temperature profiles. Based on this parametric study a formula for the critical tank diameter is developed and presented in this work. The paper concludes with recommendations on how increased wall stresses can be addressed by an appropriate design.

1. Introduction

High temperature thermal energy storage (TES) is a key element of modern concentrating solar power (CSP) plants enabling dispatchable electricity generation [1] in the multimegawatt range. State-of-the-art for thermal energy storage in CSP plants is the two-tank molten salt storage system, where hot and cold molten salt is kept in two separate tanks. Operating temperatures are between approx. 300 °C and 385 °C for parabolic trough power plants [2] and between approx. 300 °C and 560 °C for solar tower power plants [3] reaching a capacity of typically one thousand but also several thousand megawatt-hours. Molten salt storage is the most widely used grid-connected thermal energy storage system commercially, with a total installed capacity of 491 GWh

worldwide as of today [4]. Besides its use in CSP, molten salt storage is proposed for the use in conventional thermal power plants as well [5–10]. Molten salt thermal energy storage represents an exceptionally cost-effective solution for the storage of substantial quantities of energy [11]. Using molten salt as a storage medium offers several benefits, including the ability to use large, non-pressurized tanks and the versatility that arises from the salt's dual function as both a storage medium and a heat transfer fluid (HTF). Furthermore, nitrate molten salt is non-toxic and non-flammable.

In order to increase the temperature to obtain higher power cycle efficiencies, a substantial corpus of research has been conducted in the field of thermal energy storage at temperatures exceeding 600 °C, underscoring the necessity for thermal energy storage at such elevated

temperatures in industrial applications. Recent studies propose storage technologies such as latent packed beds (>600 °C), alumina packed beds (700 °C), chloride salts (800 °C), solid particles (1000 °C), liquid silicon (2000 °C) and graphite (2400 °C) [12–16]. Furthermore, ongoing developments in the field of nitrate salt are aimed at increasing the maximum temperature to over 600 °C [17,18]. It is notable that these advancements seek to achieve this increase without modifying the salt composition from the current state-of-the-art. This temperature increase could result in higher power block efficiencies and a higher storage density due to higher sensible heat per volume (higher temperature difference between hot and cold tank).

In an ideal system the hot and cold tanks are kept at an almost homogeneous temperature (in real systems, considerable temperature fluctuations in space and time can be observed). For charging, salt is pumped out of the cold tank, heated by the process and then stored in the hot tank. For discharging the process is reversed. For most of the plants, the overall salt volume is about half of the total tank volume of the two tanks; thus, one tank is always empty when fully charged or discharged, although some tanks might have a considerable sump volume (lower portion of the salt in the tank that cannot actively be used for energy storage). A desired improvement to reduce capital costs, heat losses and space requirements is the use of one single tank, which is fully filled with salt [3]. This single tank contains three characteristic zones during operation: the hot zone at the top, the cold zone at the bottom and a zone in between with a temperature gradient, the thermocline zone. The temperature profile is being formed due to external operating conditions. Since the thermocline expands over time due to convective mixing [19] and heat conduction, this zone must be extracted from the storage tank at least partially at regular intervals to keep the stratification compact and thus minimize the amount of salt at an unusable intermediate temperature. The extraction process of the thermocline zone is of paramount importance for the compactness of the thermocline zone [20–22]. During the end of a charging or discharging process, the temperature of the returning liquid from the storage increases or drops, respectively. The further a storage is charged or discharged, the steeper the temperature profile becomes in the subsequent cycle. There are different approaches as to how such a tank can be constructed.

In the thermocline storage (TC) the salt is naturally stratified due to density differences, where hot salt resides above the cold salt. A thermocline thickness of below 1 m could be demonstrated after 24 h of standby in a 2.2 m diameter tank at temperatures from 290 °C to 550 °C for this concept [23]. In the single-tank storage tank with moving barrier (TCMB) there is a physical barrier between the hot zone and the cold zone, which moves up and down when charging and discharging the tank [24,25]. The aim of this approach is to minimize the need to extract the thermocline and to realize a compact design with little unused salt. In the thermocline storage tank with filler (TCF) [26], a low-cost solid filler material is used to replace a large part of the more expensive salt. For example, the filler may be a packed bed or stackable porous bricks.

In particular, the cost reduction potential of the single-tank concepts becomes apparent if no additional tanks need to be reserved for filling, maintenance or emptying. In light of recent tank failures in the hot tank, some engineering companies and CSP operators debate the necessity of a second tank for maintenance reasons in the single-tank concept, ultimately reducing or eliminating the cost reduction potential. This study is predicated on the assumption that future tank failures can be avoided, thereby allowing the usage of only a single tank for the single-tank concept.

The worldwide largest single-tank concept at a temperature of 560 °C was demonstrated in the Test Facility for Thermal Energy Storage in Molten Salts (TESIS) with a capacity of 4 MWh [27]. For a commercial application of any of the three concepts the technology must be scaled up by one to three orders of magnitude. Unfortunately, larger dimensions automatically come along with a higher thermal deformation.

All three approaches, TC, TCMB and TCF, have in common that the tank shell is subjected to an axial temperature profile which moves up and down during charging and discharging. This has the consequence that the tank shell expands more in the upper part of the tank due to the thermal expansion of the steel than in the lower part (see Fig. 1). Additional thermally induced bending stresses therefore occur in the region of the thermocline. As a result, there may be technical limits to the diameter or width of the thermocline.

As shown in the following literature overview, research on thermocline concepts is dominated by thermodynamic modelling approaches, system simulations, material analysis and investigations on stress due to packed bed settlements. The latter is also referred to as thermal ratcheting and is not addressed in this study since it has been discussed in numerous other works [28–38]. Thermally induced bending stresses in the tank wall have so far only been investigated for cryogenic applications. For high temperature applications like molten salt, research related to thermally induced bending stresses focused on small scale structures like receiver tubes, pipes as well as thick-walled reactors.

Induced bending stresses in thin-walled structures were especially examined for large dimensions of >30 m in diameter and high temperature gradients during air preheating of two-tank storages in CSP plants for commissioning. To our knowledge there is no published work available on the analysis of wall bending stresses in single-tank systems with thermal stratification and temperature differences reaching several hundred Kelvin during operation. This aspect is of crucial importance for the feasibility and conceptional design of the single-tank TES technology in the multimegawatt hour range. Moreover, the scalability of the single-tank concept has not been addressed in any other studies known to the authors, despite its critical importance. The aim of this study is to evaluate technical limits for the upscaling of single-tank storage tanks, which result from the additional thermal stress component compared to the two-tank storage tank. For this purpose, several parameters are varied with the help of a simplified model. The aim of this paper is the development, validation and technological application of a new simplified model. The simplified model calculates the occurring maximum stresses in the tank shell with sufficient accuracy and at low computational effort. The aim of the simplified model (named model E here) is to be able to carry out specific parameter variations without having to create complex geometries and computationally intensive calculations. A validation of this model is done with the help of two experiments found in the literature. Further verification of the simplified model is performed by means of FEM simulations. After that, results of maximum possible tank diameter as a function of the thermocline thickness and required tank wall thickness as a function of the tank diameter and thermocline thickness are presented. The paper concludes with five design parameters aimed at addressing bending stresses in the tank shells of single tanks.

The paper's originality lies in its comprehensive approach to addressing the challenges of thermal stress in single-tank TES systems, the development of a simplified yet accurate model for stress
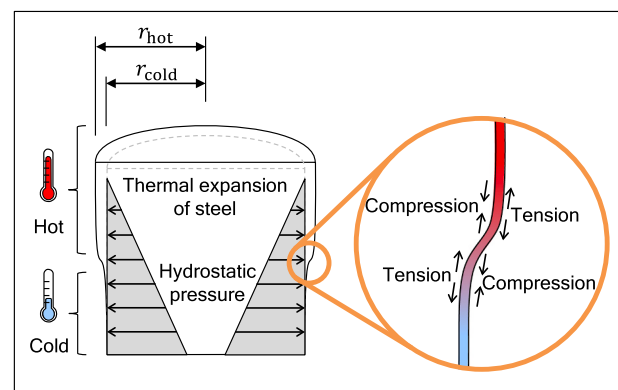

Fig. 1. Simplified scheme of thermal deformation in single-tank storage concepts related to thermal cycling of the tank wall.

calculation, and the provision of practical design guidelines for large-scale implementations. This research addresses a gap in the existing literature on the above-mentioned thermal bending stresses in tanks and offers valuable contributions to the scaling of molten salt TES technology.

2. Literature overview and fundamental background

2.1. Structural design aspects of two-tank molten salt systems

According to the NREL report on best practices in CSP [39] all accomplished and currently developed CSP projects in the United States, Europe and Africa with central receiver technology use API 650 [40] and ASME Section II [41] as a guideline for the design of the two tank storage. Nonetheless, tank failures have occurred. The authors concluded that besides foundation settlements, cyclic non-uniform thermal expansion in the bottom plates and tank wall might have been the cause for some of the reported hot tank incidents. This nonuniformity can arise from multiple effects, e.g. tank edge cooling [42–44] or temperature fluctuations of the inflowing salt [45]. Osorio et al. identified low-cycle fatigue, stress relaxation cracking, creep and buckling as the major failure behaviors in hot molten salt tanks [46]. The authors concluded that these behaviors were mainly influenced by design, fabrication, and operation factors such as: wrong design and fabrication of the floor, insufficient weldments, wrong welding electrodes, insufficient salt mixing during operation leading to temperature gradients in the tank floor, insufficient friction distribution between tank floor and foundation and operational challenges.

Some studies on the structural design of the hot tank of a two-tank storage have been published. Zeng et al. conducted a detailed strength and creep-fatigue analysis of a hot molten-salt storage tank under four different load assumptions using FEM [47]. The highest stress was observed on the inside of the bottom plate near the wall junction. Liu et al. investigated the preheating procedure of a hot tank with hot air [48]. Highest local thermal stress was found to be at the joint of the wall and the bottom plates of the tank, resulting from thermal gradients within the tank structure. The local temperature differences that caused a maximum stress of approximately 100 MPa were in the range of only 20 Kelvin. Following the investigations of Gabrielli et al. [49], Ladkany et al. [50] proposed an optimal tank design consisting of a carbon steel shell, an internal insulation layer and a stainless steel liner. Main challenges for the structural design were identified to be the unhindered thermal tank expansion as well as bending stress in the bottom region of the tank wall.

2.2. Structural design aspects of single-tank systems

In the single-tank concepts there are two additional stress mechanisms that arise due to thermal cycling of the wall: thermal deformation (Fig. 1) and thermal ratcheting.

Thermal ratcheting describes the obstruction of free tank contraction due to thermally induced cyclic packed bed settlements. It has been the focus of numerous studies on TCF storage [28–38]. The effect of thermal ratcheting is beyond the scope of this paper.

The effect of thermal deformation is present in all three TC, TCF and TCMB storage systems and hence examined in detail in this study. Thermal deformation of the tank wall occurs under constant internal pressure and temperature gradient over the height. The difference in radial expansion (defined as r_{hot} minus r_{cold}, see Fig. 1 top) is proportional to the tank diameter and the temperature difference between the hot and cold zone. For a single tank with a nominal diameter of 35 m and a temperature difference of 270 Kelvin as an example, the difference in radial expansion becomes >8 cm. The resulting deformation as indicated in Fig. 1 results in bending moments in the wall. The bending stress is in turn also a function of the wall thickness of the tank shell and the width of the thermocline zone in the wall. Under fixed boundary

conditions for temperature profile and geometry, the wall thickness remains the only free design parameter. While the hydrostatic stress component decreases with increasing wall thickness, the stress component caused by thermal expansion increases with increasing wall thickness. Hence, the additional stress component due to thermal expansion in the single-tank storage compared to the two-tank storage cannot necessarily be resolved by increasing the wall thickness. Guo et al. conducted a study on the effect of different encapsulated phase change materials in a single tank on the creep damage in the tank wall of a single tank [51].

The following studies addressed the aspect of thermal deformation in cylindrical shells for different applications: Furuhashi et al. [52] developed analytical solutions for the stress in a cylindrical vessel induced by thermal stratification of a contained fluid and evaluated the maximum occurring stress in relation to the Biot number of the vessel wall and the length of a ramp-shaped temperature profile in the fluid. A number of authors investigated the effect of tank filling procedure on thermal stress in cryogenic storage tanks, facing the same challenges and phenomena regarding thermal deformation and wall stresses as in the high temperature single-tank storage. Kang et al. investigate the filling process of a vertical cryogenic tank numerically [53] and conducted experiments on the thermally induced deformation of the tank wall at atmospheric pressure [54,55]. It was found that maximum stress occurred when the transient temperature profile had the highest local gradients. Further it was shown that maximum thermal stress was proportional to the local maximum cooling rate or filling velocity respectively. Ma et al. developed a detailed CFD model of a cryogenic LN2 tank [56] and a cryogenic LH2 tank [57] in order to investigate the maximum thermally induced tank wall stress during tank filling. Both models were validated with the experiments from Kang et al. [55].

Compared to the summarized studies on thermal deformation in small cylindrical shells, this study focuses on large-scale tank structures and combines high hydrostatic loads, high absolute temperatures, and large thermal deformations. To the best of our knowledge, this study is the first to address the thermal deformation of the single-tank concept with molten salt. While previous single-tank concepts foresaw moderate temperature differences of e.g. 127 Kelvin [32] at moderate design temperature below 400 °C, the technical evolution of the single-tank concept investigated in this study foresees temperature differences more than twice as high and design temperatures above 560 °C. The mere change to a higher steel grade with a lower strength results in thicker walls and thus exacerbates the problem of thermal stresses.

To summarize, the aspect of thermally induced wall stresses becomes increasingly important for thick-walled large size storage tanks with large temperature differences and compact thermocline zones. So far, the design approach to solving this problem is not clear. Also, no studies were found in the literature that show whether thermal decoupling from the structurally supporting wall in the form of internal insulation is required due to thermal stratification in the salt, preventing the thermally induced stresses from becoming too large. The technological and scientific question that arises is, in what range of tank diameter and thermocline thickness can the tank wall thickness actually be used as a design parameter to keep stresses below the allowable maximum?

3. Modelling methods

Numerical methods are used for parametric investigations. The focus of the model development is on wall stresses induced by hydrostatic pressure and temperature gradients over the tank height. Thermal loads are hence approximated using a parameterized temperature profile along the tank height. Tank geometries are implemented in different detail levels with the models named A to E (Fig. 3). Thermal and hydrostatic deformation of the tank wall is computed by means of different solving methods, one is a commercial FEM software (SolidWorks); the other is the implementation and solving of the governing differential equations in Matlab. The latter is validated with the FEM model and

experimental data from literature [32,55]. Both models are compared in terms of applicability.

3.1. Definition of temperature profiles in the fluid volume and tank wall

The temperature distribution in a single-tank storage system is largely dependent on its operational parameters and the width of the thermocline is not constant over time. While numerical methods can accurately describe the temperature distribution in a single-tank system, in this study we utilize a general description of the temperature as a function of the hot and cold temperatures, the position of the thermocline and the thermocline thickness. This approach facilitates a parameter analysis and provides a more intuitive interpretation of the results. Furthermore, the explicit analytical description of the temperature distribution allows for the characterization of any type of thermocline storage with this fitting function as an approximation.

There are numerous analytical solutions for temperature distribution due to heat transfer. The simplest solution is the Gauss error function, which occurs in solutions of the heat conduction equation when boundary value conditions are given by a step function. The error-function is also used and validated by numerous authors to analytically describe the temperature profile over the tank height position $T(x)$ of a thermocline in a packed bed [55,58–60]. Although the Gaussian error function is a satisfactory approximation for numerous thermocline applications, it is prudent to verify its applicability on a case-by-case basis when examining a specific thermocline storage system. The following equation is used within this study to analytically describe the temperature distribution along the height.

$$T_{\text{Fluid}}(x) = \frac{T_{\text{hot}} + T_{\text{cold}}}{2} + \frac{T_{\text{hot}} - T_{\text{cold}}}{2} \cdot erf\left(\frac{\sqrt{\pi}}{L_{\text{TC,Fluid}}} \cdot (x - x_{\text{TC}})\right) \quad (1)$$

In this function $L_{\text{TC,Fluid}}$ is defined as the distance of the turning tangent intersections with the asymptotes of the function (hot and cold temperature) as displayed in Fig. 2. The parameter x_{TC} is the vertical position of the thermocline zone.

The temperature profile in the wall can be assumed analogously to Eq. (1), representing the worst case for the thermal deformation of the wall. The real temperature distribution due to the better heat conduction of the steel can be smoother. To estimate the length $L_{\text{TC,Wall}}$ as a function of the length $L_{\text{TC,Fluid}}$, the energy balance of the wall was solved in steady state with h_{Inside}, λ_{Wall} and t_{Wall} being the heat transfer coefficient to the salt, the thermal conductivity of the wall and the wall thickness (Eq. (2)), respectively. It is further assumed that the wall is adiabatic to the outside ($h_{\text{Outside}} = 0$ W/m2K), that the heat transfer coefficient h_{Inside} is constant and that thermal inertia of the tank wall can be neglected.

$$\frac{d^2 T_{\text{Wall}}}{dx^2} = \frac{h_{\text{Inside}}}{\lambda_{\text{Wall}} \cdot t_{\text{Wall}}} \cdot (T_{\text{Wall}} - T_{\text{Fluid}}) \quad (2)$$
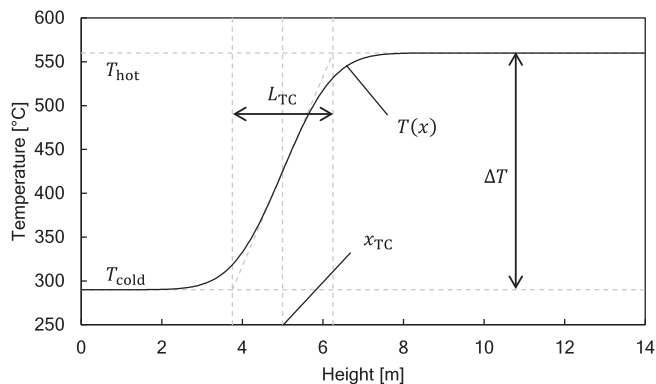

Fig. 2. Temperature profile and characteristic parameters of analytical function for temperature profile.

By integration at the mid-range position ($x = x_{\text{TC}}$) with respect to x, L_{Wall} can be expressed according to the following equation:

$$L_{\text{TC,Wall}} = \frac{1}{2}\left(L_{\text{TC,Fluid}} + \sqrt{\frac{8 \cdot \pi \cdot \lambda_{\text{Wall}} \cdot t_{\text{Wall}}}{h_{\text{Inside}}} + L_{\text{TC,Fluid}}^2}\right) \quad (3)$$

3.2. Definition of boundary conditions and models

The tank (case A) was modelled on four different levels of detail (B-E) that were compared with each other. In the context of a broad parameter study, the maximum occurring stress, calculated with a simplified model E, represents a key parameter. The hypothesis is that this maximum stress is consistent across all models under consideration. In order to validate the models, four separate models must be compared with two different experiments and with each other. The four different structural tank models and the corresponding assumptions are displayed in Fig. 3. The case A describes the real tank closely with three dimensional thermal and hydrostatic loads. There are several additional aspects relevant to tank design like deadweight, wind, earthquake, internal over- and under-pressure and snow. These aspects are neglected in the simplified model B.

Due to the axis-symmetric load profiles, the three-dimensional case A can be reduced to model B assuming a pie slice of the tank that is implemented in FEM. By isolating the region of highest expected stress in the tank shell, it is possible to further reduce the model to a one-dimensional model C. The described dimensions are reduced to radial displacement as a function of x. As will be shown later, the maximum stress occurs in the bottom region. Hence, in model C, it is further assumed that the wall-roof junction has no effect on the maximum stress and therefore the wall is assumed to be infinitely high. In model D the junction to the base plate is additionally torque free. In model E it is further assumed that the maximum stress occurs in the bottom course of the tank shell so that the tank can be modelled as a cylinder with constant wall thickness t_0. The one-dimensional models C, D and E are implemented in Matlab, the two-dimensional FEM model B is implemented in SolidWorks Simulation Premium 2021.

3.3. FEM implementation of the model B SolidWorks Simulation Premium

The FEM model B is defined by a 10-degree segment of the tank bottom and tank shell. Rotational symmetry conditions are set. The wall thickness of the shell courses and the bottom as well as material properties of the steel are set to the values given in Table A3. The temperature profile and the hydrostatic pressure are applied as the loads. It is assumed that the tank bottom lays on a stiff, frictionless and non-penetrable foundation. A mesh study was conducted to identify an optimal mesh element size. Based on the findings, the element size of the mesh was selected to be 100 mm with no local refinement. The type of solver used was Direct Sparse and automatic.

3.4. Matlab implementation of the model C to E

3.4.1. Thermal and hydrostatic deformation
Different thermal expansion along the axis of the tank primarily leads to bending stresses in axial direction. While the radius r of the tank, the temperature T and the pressure p are directly proportional to the radially outward displacement u in a sufficient vertical distance of the thermocline, the wall thickness t influences also the rigidity D and the parameter β that have an impact on the degree of bending.

The stress in a cylindrical shell with an inner radius of r and a wall thickness of t can be described by the following differential equation [61]:

$$\frac{d^2}{dx^2}\left(D\frac{d^2 u}{dx^2}\right) + 4 \cdot D \cdot \beta^4 \cdot u = p + \frac{E \cdot t \cdot \alpha}{r} \cdot (T - T_0) \quad (4)$$
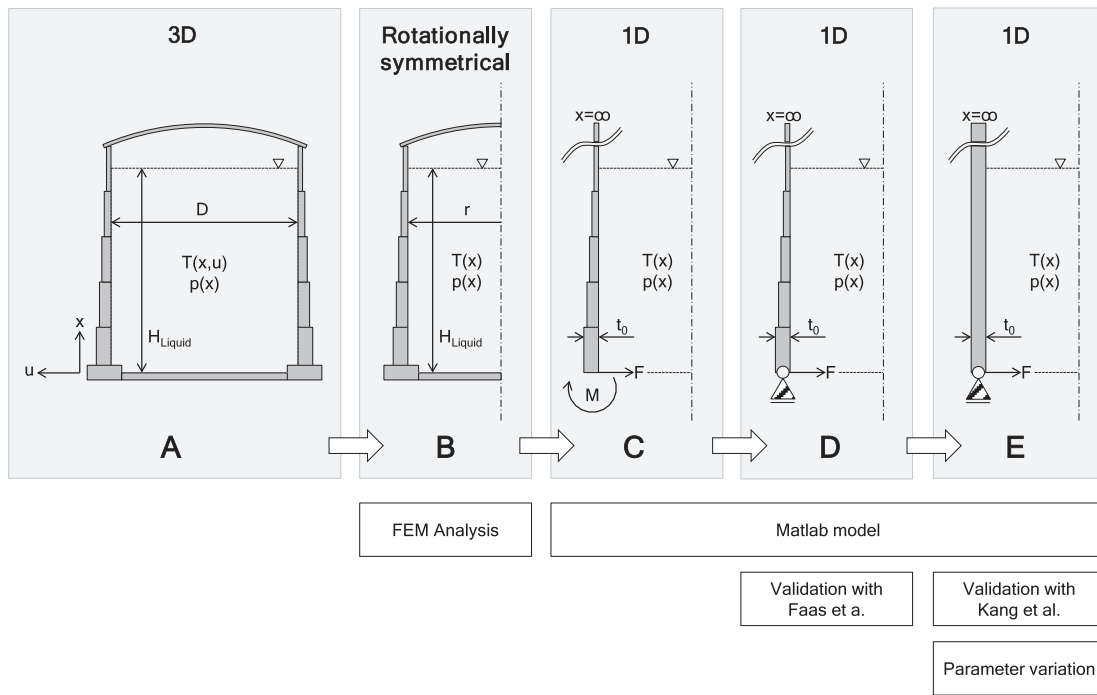
Fig. 3. Boundary conditions for case A and structural tank models B to E.

The flexural rigidity D, the parameter β, the pressure p, the wall thickness t, the radially outward displacement u, the Young's modulus E, the thermal expansion coefficient α and the temperature T are a function of the vertical position x. The Poison's ratio ν and the tank radius r are constant. The variables D, β and T_0 are defined in Eqs. (5) to (7) [61]:

$$D = \frac{E \cdot t^3}{12 \cdot (1 - \nu^2)} \tag{5}$$

$$\beta = \frac{(3 \cdot (1 - \nu^2))^{\frac{1}{4}}}{\sqrt{\frac{D}{2} \cdot t}} \tag{6}$$

$$T_0 = T|_{x=0} \tag{7}$$

This boundary value problem can be solved numerically using a finite difference code implemented in the Matlab function 'bvp4c'. This function uses the three-stage Lobatto IIIa formula [62,63]. Therefore, the fourth-order boundary value problem $u'''' = f(u)$ was transformed into a first-order boundary value problem $y' = f(y)$ using vector notation with y being a four-element vector. For this purpose, u was replaced with the first vector-element $y(1)$ in Eq. (4). By rearranging this equation, u'''' is obtained and inserted as the fourth vector-element of y'. The complete vector y' is then defined as shown in Eq. (8).

$$y' = \begin{pmatrix} y(2) \\ y(3) \\ y(4) \\ u'''' \end{pmatrix} \tag{8}$$

The radially outward displacement u could then simply be accessed from $y(1)$ after solving the first-order boundary value problem in Eq. (8).

3.4.2. Difference between the models C to E

For solving a fourth-order boundary value problem four boundary conditions must be defined. The only difference between the three models lies in the boundary conditions and geometry definition (see Table A1). In all models the radial outward displacement at the bottom of the wall is set to zero assuming a perfectly rigid base plate in radial direction having the temperature T_0. For model C the moment between

the base plate and the tank wall is calculated with the aid of model B (FEM). In the other two models D and E the connection to the base plate is considered moment free, hence the second derivative u'' becomes zero. The last two boundary conditions were specified under the assumption of an infinitely high tank wall with no external forces or moments at a position $x \gg H_{\text{tank}}$. Consequently, here the first and second derivative u' and u'' becomes zero.

3.4.3. Stress calculation

In all models C to E the radial temperature distribution is neglected. Also, effects of plate buckling are considered to be of little to no relevance. Hence the three stress components, i.e. vertical bending stress σ_{xb}, horizontal membrane stress σ_{hm} and horizontal bending stress σ_{hb}, can be calculated as follows [52]:

$$\sigma_{xb} = 6 \cdot D / t^2 \cdot \ddot{u} \tag{9}$$

$$\sigma_{hm} = E \cdot (u / r - \alpha \cdot (T - T_0)) \tag{10}$$

$$\sigma_{hb} = \nu \cdot 6 \cdot D / t^2 \cdot \ddot{u} \tag{11}$$

The vertical tensile stress is also neglected, since it only results from the vertical pressure component at the tank wall and from its own weight. The deflections are relatively low, so that vertically acting outer forces can be neglected. Any shear stress is completely neglected. Hence the von-Mises-stress is calculated as follows [64]:

$$\sigma_{\text{vMises,outside}} = \sqrt{\sigma_{xb}^2 + (\sigma_{hm} - \sigma_{hb})^2 + \sigma_{xb} \cdot (\sigma_{hm} - \sigma_{hb})} \tag{12}$$

$$\sigma_{\text{vMises,inside}} = \sqrt{\sigma_{xb}^2 + (\sigma_{hm} + \sigma_{hb})^2 - \sigma_{xb} \cdot (\sigma_{hm} + \sigma_{hb})} \tag{13}$$

Flat bottom tanks that are not subjected to high temperature gradients are generally designed with a multistage approach. The primary aspect is the selection of a minimum required wall thickness using the maximum allowed membrane stress as a criterion. Secondary aspects include wind load, earthquakes, connections between the bottom plate and the wall sheath or the wall sheath and the roof, and so forth [40]. It is not critical per se that static bending stresses, for example those

resulting from secondary aspects, exceed the plasticity limit at a surface, as they are self-limiting. Consequently, surface stresses usually have higher stress limits than membrane stresses. Therefore, for the design of a single-tank, it is proposed that the membrane stress be considered as the primary aspect. In addition to the purely static analysis, a fatigue analysis is necessary for high-cycle thermal energy storage applications, which considers all the other secondary aspects. The von-Mises-stress is only used for model validation in this study. For parameter variation, the membrane stress (σ_{hm}) is selected as a criterion. Selecting the membrane stress over surface stresses enables the identification of unfeasible single-tank configurations before detailed calculations are required. The question of whether membrane or surface stress should be regarded as the critical criterion must be answered on a case-by-case basis.

3.5. Validation method of the Matlab models D and E

Two cases from literature were chosen for the validation of the model with experimental data. The first case is the thermocline filler storage of the Solar One project [32,65] which was filled with 78 % sand and rocks and 22 % thermal oil. The selection of measurements (December 1982) was based on the requirement that thermal ratcheting had not yet occurred and that the storage had only been operated for few cycles, in order to make it comparable to the described structural tank model D (information on bending moment in the bottom edge were not accessible, so that model C could not be applied). The authors found that the dominating stress was due to hydrostatic pressure. Table A2 summarizes the data taken from literature for model validation. Fig. 4 and Fig. 5 show the comparison of the computed maximum occurring stress in the tank wall structure with the measured data of the experiments.

The second experiment used for validation is that of Kang et al. [55] where a vertical cylindrical vessel was subjected to a transient temperature profile, which is established by filling with liquid nitrogen. The authors found that the dominating stress was due to thermal deformation, since the wall material encounters a very high temperature gradient at the gas-liquid boundary. Table A2 also summarizes the main boundary conditions that were used for model validation.

3.6. Definition of a reference case for model comparison

For a comparison of the models, a single-tank reference case was defined. The dimensions are based on the hot tank of a two-tank system with 1000 MWh. The material properties for this reference case are listed in Table A3. Typical steel values for the steel grade 347H were selected for the tank wall. Since the total mass of salt in the storage remains constant irrespective of the temperature, the maximum
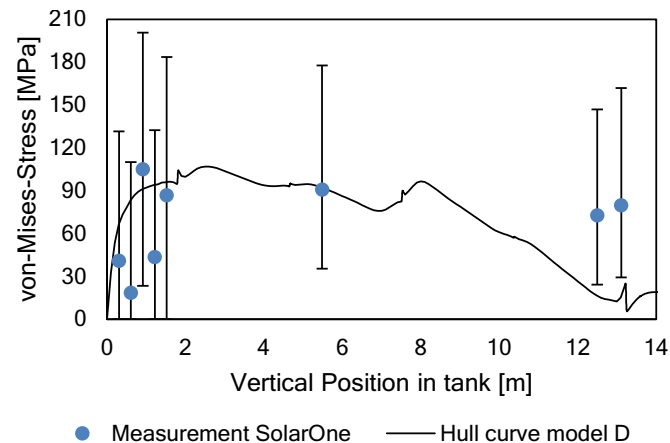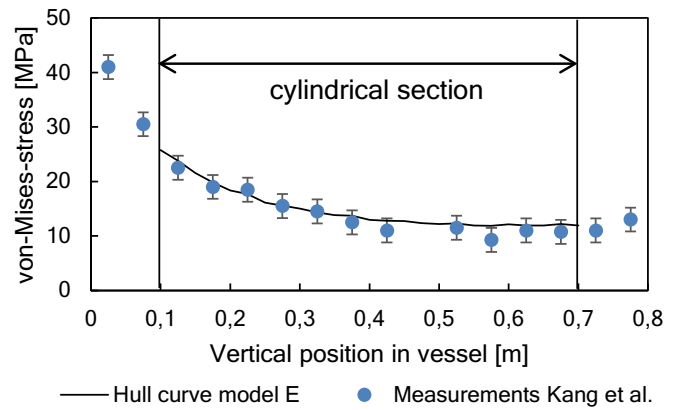
Fig. 5. Validation for model E with measurements from Kang et al.

hydrostatic pressure does not depend on temperature either. For this reason the density of Solar Salt was calculated at a constant reference temperature of 560 °C [66] resulting in the highest liquid level. For higher operating temperatures the reference temperature was not extrapolated, instead the same reference temperature was chosen.

Current molten salt tanks are limited in height by the available length of the pump shaft, reaching from above the tank roof down to the bottom of the tank and having the pump's impeller at the bottom. Typically, commercial tanks have a maximum wall height of about 14 m at the time of writing. The tank diameter is limited by the wall thickness resulting primarily from the hydrostatic pressure. Allowable wall thicknesses depend on the design code. Based on the experience from engineering projects and tank manufactures it is known that tanks with >40 m in diameter have been realized with tank walls reaching 65 mm in thickness. Although the calculated max. Position of thermocline $x_{TC,Wall,max}$ is greater than the liquid level and even the tank wall height, the temperature distribution function for $T_{Wall}(x)$ is only evaluated up to the maximum tank wall height of the corresponding model.

3.7. Method of the parametric study with model E

Tank height, liquid level as well as material properties are used from the reference case. Two parametric studies were set up for two different maximum operating temperatures. One is for a single-tank storage operating between 290 °C and 560 °C in compliance with the state of the art two tank system (case 1). The other is for a single-tank storage with elevated maximum temperature operating between 290 °C and 620 °C (case 2). The aim of these parametric studies was to identify a reasonable tank size for the single-tank. The only independent design parameters are the thermocline thickness in the wall and the wall thickness itself. In this study the required tank wall thickness was calculated for each value of tank diameter and thermocline thickness for a given allowable stress. The allowable stress was chosen according to the minimum value of either the yield strength $R_{p0.2}$ or the creep strength for 200,000 h $R_{u,200000h}$ at the corresponding design temperature reduced by a safety factor of 1.5 for the yield strength and 1.25 for the creep strength (like proposed in [67]), see Eq. (14). The design temperature was assumed 20 Kelvin higher than the maximum operating temperature of the storage. Since there was no complete set of property values available for the material 1.4550 (steel 347H), the values for the material 1.4961, which has a similar composition, were assumed. For a design temperature of 580 °C the yield strength is higher than the creep strength. Hence, the value $R_{p0.2}$ is 115 MPa [68]. For a design temperature of 640 °C the creep strength is higher than the yield strength. Hence, the value $R_{u,200000h}$ is 61 MPa [69]. The effect of cyclic load leading to fatigue was not examined in this study.

$$\sigma_{Design} < min(R_{p0.2}/1.5; R_{u,200000h}/1.25) \tag{14}$$

Fig. 4. Validation for model D with measurements from Solar One with large uncertainty values (maximum von-Mises-Stress in the wall calculated from vertical and horizontal strain measurements in December 1982).

To determine the required maximum tank diameter, the maximum membrane stress was evaluated for an equally distributed set of tank diameters between 5 m and 50 m using Eq. (12). From this set of values, the required diameter D_{tank} was interpolated linearly. Variable parameters for the parametric study are listed in Table A3.

4. Results and discussion

This study examines the impact of thermal stress on the structural integrity of single-tank thermal energy storage systems. We begin by estimating the temperature profile within the tank wall and then validating our structural mechanical models against experimental data. Thereafter, we compare the simulation results for the different simplified structural models to analyze their suitability for identifying maximum occurring wall stresses. Our parametric study then examines the effects of varying design parameters on the required wall thickness and critical tank diameter. Based on these results, we conclude with a discussion of potential strategies for scaling up single-tank systems.

4.1. Estimation of the temperature profile in the wall

To estimate how much the two lengths L_{Fluid} and L_{Wall} differ, L_{Wall} is evaluated for different values of h_{Inside}, L_{Fluid} and t_{Wall} in the following Table 1 using Eq. (3). As wall material, stainless steel is assumed ($\lambda_{Wall} = 15$ W/(mK)). Determining the local heat transfer coefficient between salt and wall requires fluid dynamic simulations or experiments which are not part of this study. That is why multiple different values for h_{Inside} were evaluated. The heat transfer h_{Inside} for direct contact between tank wall and molten salt was calculated to be between 10 and 100 W/m^{2}K based on Nusselt correlations for natural convection. Achieving a lower heat transfer can be realized with internal insulation of the wall. An internal insulation material with $\lambda_{Iso} = 0.04$ W/(mK) was assumed between the storage material and the inside of the steel tank to calculate the required insulation thickness $t_{Iso,required}$.

4.2. Validation for models D and E

Fig. 4 shows the comparison of the computed maximum occurring stress in the tank wall structure with the measured data of the experiments. The region of the semi-spherical heads (0 to 100 mm and 700 to 800 mm) was excluded from the comparison, since here obviously the modelling differs from the experimental setup.

The reported uncertainty of the measurement data of the Solar One project is in the same range as the measurement itself. Nonetheless the calculated distribution of maximum occurring stress for a traversing thermocline is within the error bounds in the bottom and middle region of the tank. The calculated stress in the top region of the tank is lower than the measured stress. As stated before, this part of the tank is not considered critical from a thermal stress perspective. The deviation is assumed to come from the roof-wall connection which is not part of the model D.

The measurements of the experiment conducted by Kang et al. exhibited minimal uncertainty. The model demonstrated satisfactory consistency with the experimental results. However, the boundary impact zone in the lower region could not be validated due to the absence of a flat bottom plate in the experiment (semi-spherical heads were used instead).

The divergent trajectories of the hull curves observed in the two experiments can be attributed to the markedly disparate temperature profiles of the two experiments. Kang et al. investigated the filling process of a cryogenic container, characterized by a pronounced temperature gradient in the lower region, which gradually diminished towards the upper area. In contrast, Faas et al. examined a thermocline storage tank, exhibiting comparable temperature gradients at the top and bottom. The reduction in stress observed in the lower section of the storage tank can be attributed to the connection between the bottom plate and the tank wall. This phenomenon is characteristic for typical flat-bottom tanks.

4.3. Simulation results and model comparison for the reference case

FEM simulation (Model B) of the reference case revealed a deformation (see Fig. 6) similar to that indicated in Fig. 1. The displayed deformation profile of a pie slice shaped cutout of the tank geometry is for the case of a thermocline position of $x_{TC} = 5$m.

The resulting maximum stress for the described model B (solid squares in Fig. 7) is compared to the maximum stress calculated with the Matlab model C (red, blue and orange solid lines in Fig. 7) for multiple thermocline positions, three of which are shown (3 m blue, 5 m red, 10 m orange).

The models D and E are also evaluated at multiple thermocline positions and compared against each other. For the three exemplary thermocline positions, model B and C show good consistency in the region of temperature impact. It can further be seen that the temperature fluctuation only has local impact on stress. Compared to the pure hydrostatic case, which is also displayed in the diagram, the stress curve along the tank wall is characterized by a peak in the lower part of the thermocline. In the upper part of the thermocline the stress at the
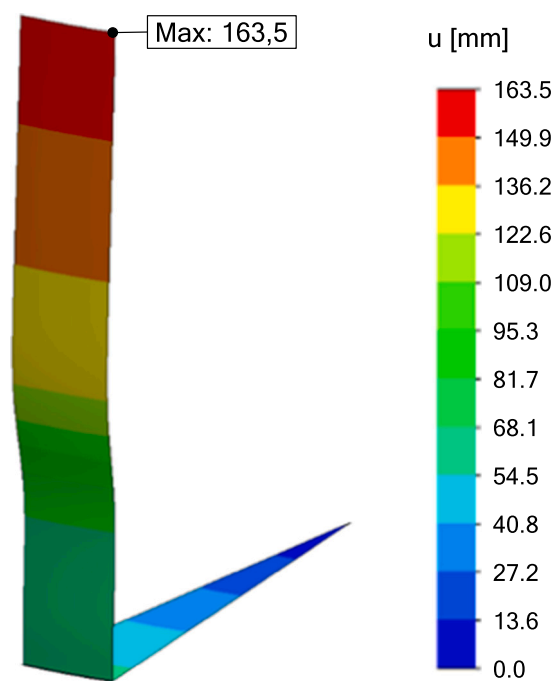
Table 1
Results for approximated thermocline length in tank wall L_{Wall} for different fluid thermocline length $L_{Fluid} = 0$ m/1 m/2 m, $\lambda_{Iso} = 0.04$ W/(mK), $\lambda_{Wall} = 15$ W/(mK)

		Direct contact between tank and fluid		Internal insulation	
$h_{Inside} =$		100 W/m^{2}K	10 W/m^{2}K	1 W/m^{2}K	0.1 W/m^{2}K
$t_{Iso,required} =$		n.a.	n.a.	0.04 m	0.4 m
t_{Wall}	0.02 m	0.1 m / 1.0 m / 2.0 m	0.4 m / 1.2 m / 2.1 m	1.4 m / 2.0 m / 2.7 m	4.3 m / 4.9 m / 5.5 m
	0.04 m	0.2 m / 1.0 m / 2.0 m	0.6 m / 1.3 m / 2.2 m	1.9 m / 2.5 m / 3.2 m	6.1 m / 6.7 m / 7.2 m
	0.08 m	0.3 m / 1.1 m / 2.0 m	0.9 m / 1.5 m / 2.3 m	2.7 m / 3.3 m / 3.9 m	8.7 m / 9.2 m / 9.7 m

Fig. 6. Deformation of tank wall u for the reference case calculated with model B at 560 °C. Deflection exaggeration by a factor of 11.4, position of thermocline $x_{TC} = 5$m.
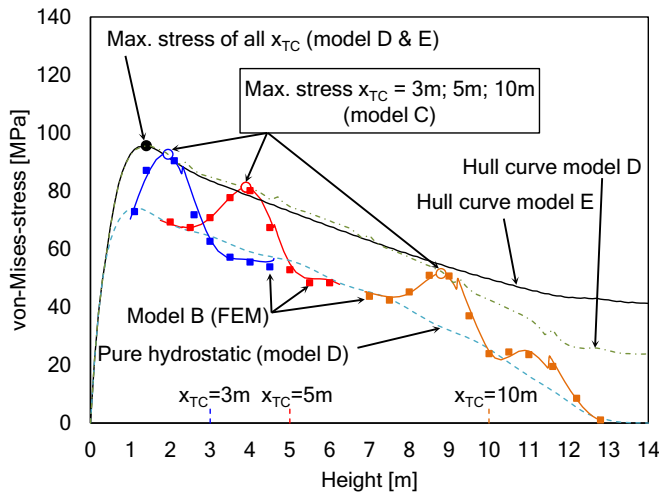
Fig. 7. Comparison of the von-Mises-Stress of the models B, C, D and E for dynamic operation at 560 °C.

outside surface even becomes lower than in the pure hydrostatic case. The influence is negligible when a sufficient distance is maintained from the thermocline zone. This can be seen by the coinciding curve of the edge area of the curve of model B with the pure hydrostatic curve. For reasons of clarity, only the curves for Models B and C are shown with regards to deviations from the hydrostatic case, in order to ascertain the position and height of maximal stress. Evaluating the stress distribution for all thermocline positions further leads to the displayed hull curves for maximum stress with models D and E, which represents the dynamic conditions of operation. It can be observed that the maximum stress of models D and E occurs at the same position with the same intensity in the relevant lower part of the tank (<8 m) with higher stress values. In the upper part of the model, it can be observed that model D presents lower stress values than model E. This is mainly due to the lower second moment of area (thinner wall) in the upper region of the wall in model D. This comparison shows that model E can be used for the parametric investigation regarding maximum occurring stress, which is described in the next section.

4.4. Results from parametric study

The described parametric study with model E is evaluated at the point of the maximum membrane stress σ_{hm}. As described, surface stresses are neglected in this study. However, for high cycle thermal energy storage applications, in addition to the purely static analysis, it is

necessary to perform a fatigue analysis, where the stresses on the surfaces are ultimately decisive. A fatigue analysis was not part of this study. The left part of Fig. 8 illustrates the relationship between the required wall thickness, the thermocline thickness $L_{TC,Tank}$ and tank diameter D_{Tank} at a specified steel design stress of 76 MPa. The figure presents lines of constant required wall thickness as a function of these variables. The thick black line indicates the resulting technical limit of the tank diameter (critical diameter) as a function of the thermocline thickness. The critical tank diameter was defined in this study as the limit curve of the simulation values for all wall thicknesses with the aid of a straight line from the origin. For the 560 °C single-tank the ratio between critical tank diameter and thermocline thickness is 13.5. The tank diameter can hence only be increased up to this limit without exceeding the allowed design stress. An increase in tank diameter would eventually necessitate an equalisation of the temperature profile within the wall, in order to maintain a sufficiently low stress level. The described technical limit (critical diameter) can be understood as the transition from a region where hydrostatically induced stress exceeds thermally induced stress. Since the diameters in the immediate vicinity of this straight line must be greatly reduced while maintaining the same wall thickness in order to fulfil the stress criteria, it is advisable to select a diameter with a minimum distance from the critical diameter.

The right part of Fig. 8 shows lines of constant wall thickness surcharge (WTS) for a single tank. The WTS is defined as the percentage of the required additional wall thicknesses for a single-tank with temperature gradient according to Eq. (1) in comparison to an equally sized single-tank with constant temperature T_{Hot}. The required surcharge of the tank walls depends mainly on the difference between the selected tank diameter and the critical tank diameter. The limit for WTS at the critical diameter lies slightly above 40 %; beyond this value the stress level increases again.

As an example, a single tank with a thermocline thickness of 2 m has a critical tank diameter of 27 m, thus the permitted tank diameter must be lower. For a tank diameter of 24 m (3 m less than the critical diameter) the tank wall thickness must be at least 40 % greater than for the purely hydrostatic case. For a tank diameter of 21 m (i.e. 6 m less than the critical diameter) it must be only 20 % greater and for a diameter of 17 m (7 m less) it must be only 10 % greater.

In other words, a tank with a thermocline-shaped temperature profile within the wall must be designed with 10–40 % thicker walls in order to withstand the additional loads due to thermal deformation. As the line of the technical limit is approached, the required wall thickness surcharge increases steadily. Increasing the wall thickness to compensate for thermally induced stresses is therefore of limited use.

The critical tank diameter, as drawn in Fig. 8, was evaluated for different design stresses ($\sigma_{allowed}$). The resulting lines are plotted in Fig. 9 for maximum tank temperatures of 560 °C and 620 °C. The dashed lines
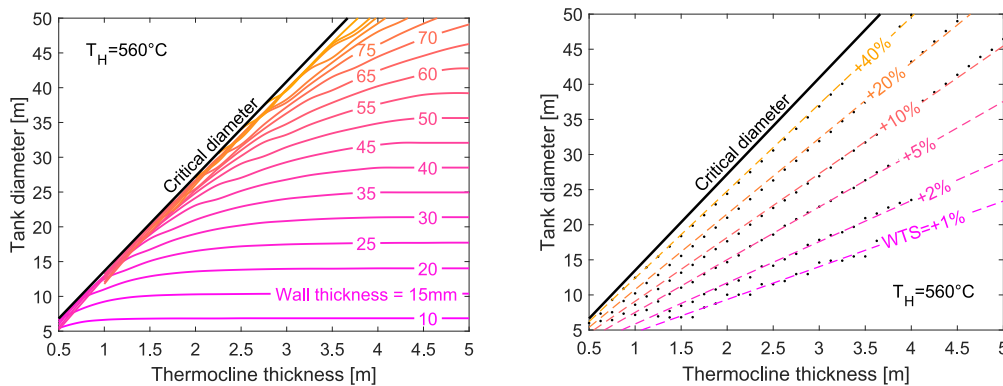

Fig. 8. Left: minimum required tank wall thickness for a maximum operating temperature of 560 °C and a design stress of 76 MPa determined with model E. Black line shows the technical limit (critical diameter); Right: wall thickness surcharge (WTS) of tank wall thickness due to thermal deformation compared to the pure hydrostatic case for a maximum operating temperature of 560 °C and a design stress of 76 MPa
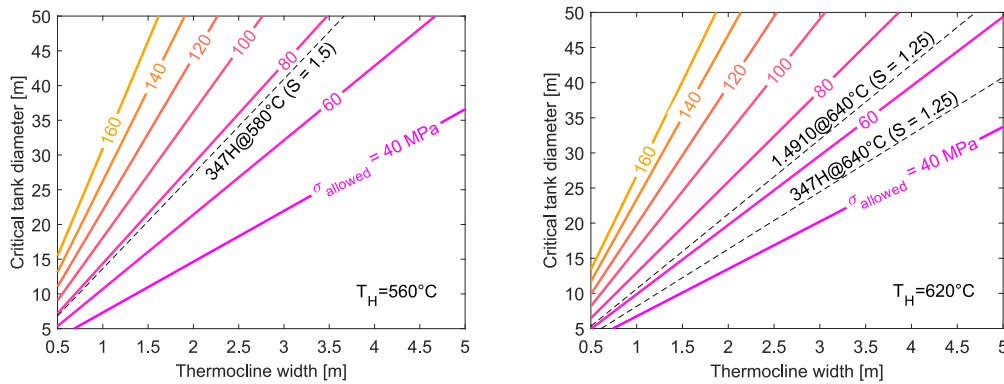
Fig. 9. Critical tank diameter as a function of the thermocline thickness for different design stresses ($\sigma_{allowed}$) at a maximum tank temperature of 560 °C (left) and 620 °C (right).

represent the critical diameter for a specific selected material at design conditions. For the 560 °C case this line is identical with the one in Fig. 10. For the 620 °C case the allowed stress of 347H is considerably reduced and consequently the critical diameter is also smaller. A possible alternative for the steel 347H is the heat resistant steel 316LN (1.4910) which was also proposed by other authors for the use in molten salt storage with elevated temperatures [70]. Further discussion will be needed on whether the allowable stress needs to be determined based on the design temperature or rather on the actual temperature at the point of maximum membrane stress. It is expected that this assumption would have a positive impact on the critical tank diameter, since the temperature at the point of the maximum membrane stress is close to the cold temperature (in this case 290 °C).

As discussed before, a temperature increase leads to a smaller slope of the critical tank diameter with respect to the thermocline thickness. This can be explained by the higher temperature difference between top and bottom (in this case from a temperature difference of 270 K to a temperature difference of 330 K) and consequently a higher thermal deformation. A sensitivity analysis of the influence of temperature difference and hydrostatic pressure resulted in the curves presented in Fig. 10. Both diagrams illustrate the ratio of the critical tank diameter to the thermocline thickness as a function of the allowed stress. In the left diagram, two additional curves are included to illustrate the sensitivity of the baseline temperature difference of 270 K to temperature differences of 210 K and 330 K. Similarly, in the right diagram, two additional curves are included to illustrate the sensitivity of the baseline hydrostatic pressure of 2.1 bar to hydrostatic pressures of 1.3 bar and 3 bar. As the allowed stress level rises, the critical diameter increases, as also illustrated in Fig. 9. An elevation in the temperature difference between the hot and cold salt results in a reduction of the critical diameter. Similarly, an increase in hydrostatic pressure (for instance, through the utilization of a denser fluid or a higher tank) also yields a decrease in the critical diameter. From these curves it can be concluded, that the

permitted stress has the biggest influence on the critical tank diameter within the selected boundaries.

The critical tank diameter $D_{critical}$ can further be approximated by a parabolic function of $\sigma_{allowed}$ in MPa using linear regression, formula (15). The parameters a and b were also calculated as a parabolic function of p_{hyd} in bar and ΔT in K by means of linear regression.

$$D_{critical} \approx (a \cdot \sigma_{allowed}^2 / \text{MPa}^2 + b \cdot \sigma_{allowed} / \text{MPa}) \cdot L_{TC} \quad (15)$$

The variables a and b are defined in Eqs. (16) and (17).

$$a = -3.187 \cdot 10^{-5} \cdot p_{hyd}^2 / \text{bar}^2 + 1.326 \cdot 10^{-4} \cdot p_{hyd} / \text{bar}$$
$$+ 1.714 \cdot 10^{-8} \cdot \Delta T^2 / \text{K}^2 - 1.208 \cdot 10^{-5} \cdot \Delta T / \text{K} + 2.024 \cdot 10^{-3} \quad (16)$$

$$b = 2.031 \cdot 10^{-2} \cdot p_{hyd}^2 / \text{bar}^2 - 1.363 \cdot 10^{-1} \cdot p_{hyd} / \text{bar}$$
$$- 1.806 \cdot 10^{-7} \cdot \Delta T^2 / \text{K}^2 - 1.167 \cdot 10^{-5} \cdot \Delta T / \text{K} + 3.823 \cdot 10^{-1} \quad (17)$$

This empirical formula can be used for the design phase of a single tank in order to make a rough estimate of the required dimensions of the tank. With the insights from Fig. 8 it is also possible to make a first estimation for the required wall thickness.

4.5. Discussion

It is concluded in this paper that there are five possible directions for the scaling up of the single-tank concept from a structural design perspective.

One possibility is to **control operation with a minimum thermocline thickness** so that the thermal stress is maintained at a low level and the tank diameter can be increased. The effect on costs and system performance has been investigated in [71]. The drawback of this approach is that larger storage tank volumes would be required, leading to a larger amount of salt that cannot be used for storing thermal energy.

Hence a viable concept is to decouple the thermocline thickness of the salt from the thermocline thickness in the tank wall by means of **internal insulation**. This has also been the focus of numerous studies in the field of molten nitrate as well as chloride salt thermal energy storage [49,50,72,73], allowing for a small thermocline thickness in the salt and even offering the possibility to use low cost carbon steel for the tank shell due to the lower temperatures. Yet, the challenge of this concept is to find an insulation material that has both a low heat conductivity at reasonable costs and good failure resistance under hydrostatic pressure and cycling temperatures.

The third option is the use of **multiple smaller single-tanks**. Besides the fact that the thermal load in the tank wall is kept low even with a low thermocline thickness, this modular approach also offers a number of system-specific advantages such as a higher utilization of the storage
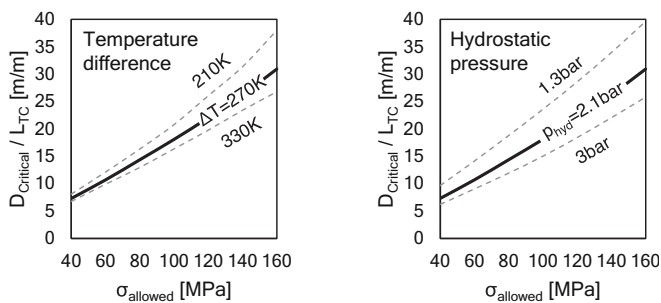

Fig. 10. Sensitivity analysis for critical tank diameter per thermocline thickness as a function of the allowed membrane stress (left: influence of temperature difference; right: influence of hydrostatic pressure)

tanks and reduced temperature fluctuations by means of mixing control as shown by Roos et al. [74] and Osorio et al. [75,76]. Whether there is also a cost benefit of using multiple smaller single-tanks rather than a two-tank system must be evaluated.

A fourth possibility is to **increase the tank height** beyond the 14 m, which have been customary until now. The single-tank concept with its always-high fluid level would likely allow for such a development, since the vertical position of the pumps is not restricted by a changing liquid level as the tank is always completely filled with salt irrespective of the charging level.

As a fifth possibility, one could examine **different structural materials** that allow higher stresses at elevated temperatures, have a lower thermal expansion coefficient or lower Young's modulus.

5. Summary and conclusion

In the present study the thermal stress of a molten salt single-tank was examined by three different numerical models with different levels of detail and with an FEM model. To our knowledge these studies represent the first work on wall bending stresses in high-temperature single-tank TES systems with thermal stratification. The three models were verified with each other and validated with two experiments. It was concluded that with regard to the maximum occurring stress the simplified numerical model E is sufficient for describing the relevant phenomena in molten salt single-tanks with a thermocline zone along with the hydrostatic pressure in the lower part of the tank. Parametric studies helped to assess the technical limit for scaling up the single-tank concept. As the most essential parameters for the design, the diameter of the tank and the thermocline thickness in the wall were examined. A dynamic operating mode was selected for the analysis of the TC tank, whereby the stress was evaluated for all potential thermocline positions during dynamic operation. This assessment was conducted for two distinct maximum operating temperatures: 560 °C and 620 °C. It was determined that, under the assumption of constant height and constant temperature difference between hot and cold salt, a critical diameter (technical limit) could be defined. The parameters of this technical limit include tank diameter and thermocline thickness. The technical limit for the tank diameter increases linearly with the thickness of the thermocline in the wall. The slope defined as the ratio between the increase in diameter and the increase in required thermocline thickness is approximately 13.5 for the 560 °C case. For the 620 °C case the slope is 8.2 or 10.6 depending on the selected steel. A sensitivity analysis further showed that the temperature difference and the hydrostatic pressure influence the critical tank diameter moderately. It is further concluded that attention should be paid especially to the correct material selection

when increasing the operating temperature. Tank material that allows for high stress values would facilitate building of larger storage tanks, which might lead to reduced capital expenses associated with the proposed single-tank storage system.

The study proposes five potential pathways for scaling up the proposed single-tank storage. These include the use of a different structural material, of an internal insulation or of multiple smaller tank units. The work particularly highlights the potential of single-tank concepts to reduce costs and minimize heat losses. It also provides insights for the design of large-scale systems. Single-tank concepts can play a major role in reducing the costs for high temperature molten salt thermal energy storage. Additional advantages include significantly lower thermal losses and lower footprints. The small volume of hot gas and its simple handling could be also an advantage. This study reveals the correlation between tank diameter, thermocline thickness and required tank wall thickness. Therefore, the developed methodology can be extended to study the impact of other parameters based on the requirements of the specific end-use applications. The outcome of this study can be directly used as a guide for the conceptual design of large molten salt single-tanks and for the anticipation of their maximum possible dimensions.

CRediT authorship contribution statement

Freerk Klasing: Writing – original draft, Visualization, Validation, Software, Methodology, Investigation, Conceptualization. **Mark Schmitz:** Writing – review & editing. **Christian Odenthal:** Writing – review & editing. **Thomas Bauer:** Writing – review & editing, Funding acquisition.

Declaration of competing interest

The authors declare that they have no known competing financial interests or personal relationships that could have appeared to influence the work reported in this paper.

Data availability

The authors do not have permission to share data.

Acknowledgement

Appendix A. Tables

Table A1
Boundary conditions for the three models C to E

Wall thickness t	Model C	Model D	Model E
	Function of x	Function of x	Constant
Boundary condition 1	$u\|_{x=0} = 0$	$u\|_{x=0} = 0$	$u\|_{x=0} = 0$
Boundary condition 2	$u''\|_{x=0}$ gotten from model B	$u''\|_{x=0} = 0$	$u''\|_{x=0} = 0$
Boundary condition 3	$u'\|_{x \gg H_{tank}} = 0$	$u'\|_{x \gg H_{tank}} = 0$	$u'\|_{x \gg H_{tank}} = 0$
Boundary condition 4	$u''\|_{x \gg H_{tank}} = 0$	$u''\|_{x \gg H_{tank}} = 0$	$u''\|_{x \gg H_{tank}} = 0$

Table A2

Boundary conditions and properties used for model validation with experiments

	Solar One	Kang et al.
Dynamic temperature profile $T(x)$	1.3 m thermocline from 177 °C to 304 °C approximated from fig. 12 in [32] traversing the complete storage	Interpolated from Fig. 7 in [55]
Hydrostatic load $p(x)$	According to Fig. 9 in [32]	According to the liquid level calculated from a constant filling mass flow of 0.08 kg/s [55]
Wall thickness $t(x)$	Profile according to Fig. 8 in [32]	Constant 3 mm [55]
Tank dimensions	Flat bottom tank with a diameter of 18.2 m and a filling level of 12.4 m [32]	Vertical pressure vessel (cylindrical part 600 mm high and 400 mm in diameter) with semi-spherical heads (125 mm high) [55]
Wall material	Carbon steel [32]	Aluminium [55]
Poison's ratio ν	0.3	0.3
Youngs modulus E	185 GPa for 300 °C [77]	75 GPa for -169 °C [78]
Thermal expansion coefficient α	10.8e-6 1/K	20e-6 1/K
Absolute uncertainty	Calculated with the theory of error propagation from a constant horizontal and vertical uncertainty of ± 56 MPa [32]	Constant ± 2.2 MPa [55]

Table A3

Tank dimensions, boundary conditions, material properties and variable parameters for reference case and parametric study

Goal	Validation and model comparison	Parametric study	
Case	Reference case	Case 1 (Base design)	Case 2 (Elevated temperature design)
Model	B, C, D, E	E	
Max. operating temperature	560 °C	560 °C	620 °C
Min. operating temperature	290 °C		
Design stress of wall material σ_{allowed}	n.a.	Varied from 40 MPa to 160 MPa	
Tank diameter D_{Tank}	24.5 m	Varied from 5 to 50 m	
Thermocline thickness $L_{\text{TC,Wall}}$	2.5 m	Varied from 0.5 to 5 m	
Position of thermocline	Varied between $x_{\text{TC,Wall},min}$ and $x_{\text{TC,Wall},max}$ resulting from $T_{\text{bottom plate},max}$ and $T_{\text{LL},min}$.		
Tank wall height H_{Tank}	14 m		
Liquid level H_{LL}	12.7 m		
Sheet thickness t_i (top to bottom)	Model B to D: $[19, 22, 25, 28, 31, 34]$ mm Model E: 34 mm	Calculated from σ_{allowed}, D_{Tank} and $L_{\text{TC,Wall}}$	
Sheet height h_i (top to bottom)	Model B to D: $[2.5, 2.3, 2.3, 2.3, 2.3, 2.3]$ m Model E: 14 m	14 m	
Bottom plate thickness $t_{\text{bottom plate}}$	Model B: 24 mm Model C to E: n.a.	n.a.	
Max. allowed temperature of bottom plate $T_{\text{bottom plate},max}$	300 °C		
Min. allowed temperature at liquid level $T_{\text{LL},min}$	300 °C		
Min./Max. theoretical position of thermocline $x_{\text{TC,Wall}}$ resulting from $T_{\text{bottom plate},max}$ and $\Delta T_{\text{LL},min}$	Min: 1.78 m Max: 14.48 m	Function of $L_{\text{TC,Wall}}$	
Young's modulus	$E = \left(2 \bullet 10^{11} - 7.29 \bullet 10^7 \bullet \dfrac{T}{°C}\right)$ Pa		
Thermal expansion coefficient	$\alpha = 18.3 \bullet 10^{-6} \dfrac{1}{K}$		
Poison's ratio	$\nu = 0.3$		
Density of fluid ρ_{Fluid}	1734 kg/m^3	1696 kg/m^3	

References

[1] R. Pitz-Paal, Concentrating solar power: still small but learning fast, Nat. Energy 2 (17095) (2017), https://doi.org/10.1038/nenergy.2017.95.

[2] U. Herrmann, B. Kelly, H. Price, Two-tank molten salt storage for parabolic trough solar power plants, Energy 29 (2004) 883–893, https://doi.org/10.1016/S0360-5442(03)00193-2.

[3] A. Gil, M. Medrano, I. Martorell, A. Lázaro, P. Dolado, B. Zalba, et al., State of the art on high temperature thermal energy storage for power generation. Part 1—concepts, materials and modellization, Renew. Sust. Energ. Rev. 14 (2010) 31–55, https://doi.org/10.1016/j.rser.2009.07.035.

[4] C. Prieto, P.D. Tagle-Salazar, D. Patiño, J. Schallenberg-Rodriguez, P. Lyons, L. F. Cabeza, Use of molten salts tanks for seasonal thermal energy storage for high penetration of renewable energies in the grid, Journal of Energy Storage. 86 (2024) 111203, https://doi.org/10.1016/j.est.2024.111203.

[5] M.K. Drost, Z.I. Antoniak, D.R. Brown, S. Somasundaram, Central station thermal-energy storage for peak and intermediate load power-generation, Energy 17 (1992) 127–139, https://doi.org/10.1016/0360-5442(92)90062-5.

[6] D. Li, J. Wang, Study of supercritical power plant integration with high temperature thermal energy storage for flexible operation, Journal of Energy Storage. 20 (2018) 140–152, https://doi.org/10.1016/j.est.2018.09.008.

[7] Q. Yong, Y. Tian, X. Qian, X. Li, Retrofitting coal-fired power plants for grid energy storage by coupling with thermal energy storage, Appl. Therm. Eng. 215 (2022) 119048, https://doi.org/10.1016/j.applthermaleng.2022.119048.

[8] B. Wang, H. Ma, S. Ren, F. Si, Effects of integration mode of the molten salt heat storage system and its hot storage temperature on the flexibility of a subcritical coal-fired power plant, Journal of Energy Storage. 58 (2023) 106410, https://doi.org/10.1016/j.est.2022.106410.

[9] B. Li, Y. Cao, T. He, F. Si, Thermodynamic analysis and operation strategy optimization of coupled molten salt energy storage system for coal-fired power plant, Appl. Therm. Eng. 236 (2024) 121702, https://doi.org/10.1016/j.applthermaleng.2023.121702.

[10] V.A. Kayayan, Are Carnot batteries an alternative when repurposing coal power plants in Europe?, in: International Renewable Energy Storage Conference (IRES 2022) Atlantis Press, 2023, pp. 3–13.

[11] H.G. Kamath, R. Majumdar, A.V. Krishnan, R. Srikanth, Cost and environmental benefits of coal-concentrated solar power (CSP) hybridization in India, Energy 240 (2022) 122805, https://doi.org/10.1016/j.energy.2021.122805.

[12] R. Majumdar, S.K. Saha, Computational study of performance of cascaded multi-layered packed-bed thermal energy storage for high temperature applications, Journal of Energy Storage. 32 (2020) 101930, https://doi.org/10.1016/j.est.2020.101930.

[13] W. Ding, T. Bauer, Progress in research and development of molten chloride salt technology for next generation concentrated solar power plants, Engineering 7 (2021) 334–347, https://doi.org/10.1016/j.eng.2020.06.027.

[14] R. Anderson, L. Bates, E. Johnson, J.F. Morris, Packed bed thermal energy storage: a simplified experimentally validated model, Journal of Energy Storage. 4 (2015) 14–23, https://doi.org/10.1016/j.est.2015.08.007.

[15] C. Amy, M. Pishahang, C.C. Kelsall, A. LaPotin, A. Henry, High-temperature pumping of silicon for thermal energy grid storage, Energy 233 (2021) 121105, https://doi.org/10.1016/j.energy.2021.121105.

[16] C.C. Kelsall, K. Buznitsky, A. Henry, Technoeconomic analysis of thermal energy grid storage using graphite and tin, arXiv preprint arXiv:210607624, 2021.

[17] C.S. Turchi, J. Vidal, M. Bauer, Molten salt power towers operating at 600–650 °C: salt selection and cost benefits, Sol. Energy 164 (2018) 38–46, https://doi.org/10.1016/j.solener.2018.01.063.

[18] A. Bonk, M. Braun, V.A. Sötz, T. Bauer, Solar salt – pushing an old material for energy storage to a new limit, Appl. Energy 262 (2020) 114535, https://doi.org/10.1016/j.apenergy.2020.114535.

[19] H. Otto, C. Naumann, C. Odenthal, C. Cierpka, Unsteady inherent convective mixing in thermal-energy-storage systems during standby periods, PRX Energy 2 (2023) 043001, https://doi.org/10.1103/PRXEnergy.2.043001.

[20] S.M. Flueckiger, S.V. Garimella, Second-law analysis of molten-salt thermal energy storage in thermoclines, Sol. Energy 86 (2012) 1621–1631, https://doi.org/10.1016/j.solener.2012.02.028.

[21] J.F. Hoffmann, T. Fasquelle, V. Goetz, X. Py, A thermocline thermal energy storage system with filler materials for concentrated solar power plants: experimental data and numerical model sensitivity to different experimental tank scales, Appl. Therm. Eng. 100 (2016) 753–761, https://doi.org/10.1016/j.applthermaleng.2016.01.110.

[22] C. Odenthal, F. Klasing, T. Bauer, Parametric study of the thermocline filler concept based on exergy, Journal of Energy Storage. 17 (2018) 56–62, https://doi.org/10.1016/j.est.2018.01.009.

[23] C. Odenthal, F. Klasing, T. Bauer, Investigation of the thermocline degradation in a molten salt storage tank, in: SolarPACES Conference 2022, 2022. Albuquerque.

[24] J. Lata, J. Blanco, Single Tank Thermal Storage Design for Solar Thermal Power Plants. SolarPACES 2010, 2010.

[25] R.J. Copeland, Method and Apparatus for Operating an Improved Thermocline Storage Unit, 1985. Medium: X; Size: Pages: v.

[26] Z. Yang, S.V. Garimella, Cyclic operation of molten-salt thermal energy storage in thermoclines for solar power plants, Appl. Energy 103 (2013) 256–265, https://doi.org/10.1016/j.apenergy.2012.09.043.

[27] C. Odenthal, F. Klasing, P. Knödler, S. Zunft, T. Bauer, Experimental and numerical investigation of a 4 MWh high temperature molten salt thermocline storage system with filler, AIP Conf. Proc. 2303 (2020) 190025, https://doi.org/10.1063/5.0028494.

[28] S. Flueckiger, Z. Yang, S.V. Garimella, An integrated thermal and mechanical investigation of molten-salt thermocline energy storage, Appl. Energy 88 (2011) 2098–2105, https://doi.org/10.1016/j.apenergy.2010.12.031.

[29] S.M. Flueckiger, Multiscale Simulation of Thermocline Energy Storage for Concentrating Solar Power [Ph.D.], Purdue University, Ann Arbor, 2013.

[30] S.M. Flueckiger, Z. Yang, S.V. Garimella, Review of molten-salt thermocline tank modeling for solar thermal energy storage, Heat Transfer Eng. 34 (2013) 787–800, https://doi.org/10.1080/01457632.2012.746152.

[31] I. González, O. Lehmkuhl, C.D. Pérez-Segarra, A. Oliva, Dynamic Thermoelastic analysis of thermocline-like storage tanks, Energy Procedia 69 (2015) 850–859, https://doi.org/10.1016/j.egypro.2015.03.106.

[32] S.E. Faas, L.R. Thorne, E.A. Fuchs, N.D. Gilbertsen, 10 MWe Solar Thermal Central Receiver Pilot Plant: Thermal Storage Subsystem Evaluation - Final Report, Sandia National Laboratories, 1986.

[33] G.J. Kolb, G. Lee, P. Mijatovic, E. Valmianski, Thermal Ratcheting Analysis of Advanced Thermocline Energy Storage Tanks. SolarPACES, 2011, p. 2011. United States.

[34] Knödler P, Dreißigacker V, Zunft S, D. L., S. Z. Packed Bed Heat Storage: Continuum Mechanics Model and Validation Using Concrete and Other Solid Storage Media in Thermal Energy Storage (TES) Systems. SolarPACES 2015 2016. p. 050024; https://doi.org/10.1063/1.4949122.

[35] V. Dreißigacker, H. Müller-Steinhagen, S. Zunft, Thermo-mechanical analysis of packed beds for large-scale storage of high temperature heat, Heat Mass Transf. 46 (2010) 1199–1207.

[36] V. Dreißigacker, S. Zunft, H. Müller-Steinhagen, A thermo-mechanical model of packed-bed storage and experimental validation, Appl. Energy 111 (2013) 1120–1125.

[37] S.M. Flueckiger, Z. Yang, S.V. Garimella, Thermomechanical simulation of the solar one thermocline storage tank, Journal of Solar Energy Engineering. 134 (2012), https://doi.org/10.1115/1.4007665.

[38] P. Knödler, Thermo-mechanical investigations of packed beds for high temperature heat storage: uniaxial compression test experiments and particle discrete simulations, Appl. Sci. 9 (2019) 1600.

[39] M. Mehos, H. Price, R. Cable, D. Kearney, B. Kelly, G. Kolb, et al., Concentrating Solar Power Best Practices Study. National Renewable Energy Lab. (NREL), Golden, CO (United States), 2020.

[40] Institute AP, API 650 - Welded Tanks for Oil Storage, Thirteenth edition, 2020.

[41] Engineers ASoM, ASME Boiler & Pressure Vessel Code. Section II – Materials, 2019.

[42] Schulte-Fischedick J, Tamme R, Herrmann U. CFD Analysis of the Cool Down Behaviour of Molten Salt Thermal Storage Systems. ASME 2008 2nd International Conference on Energy Sustainability collocated with the Heat Transfer, Fluids Engineering, and 3rd Energy Nanotechnology Conferences2008. p. 515–24; https://doi.org/10.1115/es2008-54101.

[43] C. Suárez, A. Iranzo, F.J. Pino, J. Guerra, Transient analysis of the cooling process of molten salt thermal storage tanks due to standby heat loss, Appl. Energy 142 (2015) 56–65, https://doi.org/10.1016/j.apenergy.2014.12.082.

[44] Zhou H, Shi H, Zhu Y, Fang W, C. P, R. O, et al. An Experimental Investigation of Temperature Distribution and Heat Loss in Molten Salt Tanks in Concentrating Solar Power Plants. 2020;12:014101; https://doi.org/10.1063/1.5131071.

[45] A. Iranzo, C. Suárez, J. Guerra, Mixing enhancement in thermal energy storage molten salt tanks, Energy Convers. Manag. 168 (2018) 320–328, https://doi.org/10.1016/j.enconman.2018.04.113.

[46] J.D. Osorio, M. Mehos, L. Imponenti, B. Kelly, H. Price, J. Torres-Madronero, et al., Failure Analysis for Molten Salt Thermal Energy Storage Tanks for In-Service CSP Plants. United States, 2024, https://doi.org/10.2172/2331241 p. Medium: ED; Size: 128 p.

[47] X. Zeng, X. Wang, H. Li, C. Qian, Strength and Creep-fatigue Analysis of a Molten-salt Storage Tank. 2019 International Conference on Artificial Intelligence and Advanced Manufacturing (AIAM), 2019, pp. 742–746, https://doi.org/10.1109/AIAM48774.2019.00153.

[48] X. Liu, S. Yue, L. Lu, A new method for optimizing the preheating characteristics of storage tanks, Renew. Energy 165 (2021) 25–36, https://doi.org/10.1016/j.renene.2020.11.004.

[49] R. Gabbrielli, C. Zamparelli, Optimal design of a molten salt thermal storage tank for parabolic trough solar power plants, Journal of Solar Energy Engineering. 131 (2009), https://doi.org/10.1115/1.3197585.

[50] S. Ladkany, W. Culbreth, N. Loyd, Molten salts and applications II: 565 C molten salt solar energy storage design, corrosion, and insulation, Journal of Energy Power Engineering. 12 (2018) 517–532.

[51] Y.-F. Guo, B.-C. Du, C. Xu, Y.-G. Lei, Effects of EPCM particle properties on creep damage of the molten salt packed-bed thermal energy storage system, Journal of Energy Storage. 68 (2023) 107808, https://doi.org/10.1016/j.est.2023.107808.

[52] I. Furuhashi, N. Kawasaki, N. Kasahara, Evaluation charts of thermal stresses in cylindrical vessels induced by thermal stratification of contained fluid, J. Comput. Sci. Technol. 2 (2008) 547–558.

[53] Z. Kang, L. Yanzhong, X. Mengjian, W. Lei, Investigation of the chill-down behavior and thermal stress distribution of a cryogenic tank during the filling process, Phys. Procedia 67 (2015) 342–347.

[54] M. Kang, J. Kim, H. You, D. Chang, Experimental investigation of thermal stratification in cryogenic tanks, Exp. Thermal Fluid Sci. 96 (2018) 371–382, https://doi.org/10.1016/j.expthermflusci.2017.12.017.

[55] Z. Kang, L. Yanzhong, M. Yuan, W. Lei, X. Fushou, W. Jiaojiao, Experimental study on cool down characteristics and thermal stress of cryogenic tank during LN2 filling process, Appl. Therm. Eng. 130 (2018) 951–961.

[56] Y. Ma, K. Zhu, Y. Li, F. Xie, Simulation on chill-down behavior and induced thermal stress of a cryogenic tank during LN2 filling, Appl. Therm. Eng. 181 (2020) 115876.

[57] Y. Ma, K. Zhu, Y. Li, F. Xie, Numerical investigation on chill-down and thermal stress characteristics of a LH2 tank during ground filling, Int. J. Hydrog. Energy 45 (2020) 25344–25356, https://doi.org/10.1016/j.ijhydene.2020.06.056.

[58] A. Cabelli, Storage tanks—a numerical experiment, Sol. Energy 19 (1977) 45–54, https://doi.org/10.1016/0038-092X(77)90087-1.

[59] H. Yoo, E.-T. Pak, Analytical solutions to a one-dimensional finite-domain model for stratified thermal storage tanks, Sol. Energy 56 (1996) 315–322, https://doi.org/10.1016/0038-092X(96)89365-0.

[60] R. Bayón, E. Rojas, Analytical function describing the behaviour of a thermocline storage tank: a requirement for annual simulations of solar thermal power plants, Int. J. Heat Mass Transf. 68 (2014) 641–648, https://doi.org/10.1016/j.ijheatmasstransfer.2013.09.070.

[61] S. Timoshenko, S. Woinowsky-Krieger, Theory of Plates and Shells, McGraw-Hill, 1959.

[62] J. Kierzenka, L.F. Shampine, A BVP solver based on residual control and the Maltab PSE, ACM Trans. Math. Softw. 27 (299–316) (2001), https://doi.org/10.1145/502800.502801.

[63] L.F. Shampine, J. Kierzenka, M.W. Reichelt, Solving Boundary Value Problems for Ordinary Differential Equations in MATLAB With bvp4c, MATLAB File Exchange, 2004.

[64] S. Timoshenko, Strength of Materials Part 1. D, Van Nostrand Co., Inc, 1940.

[65] G.J. Kolb, D.J. Alpert, C.W. Lopez, Insights from the operation of Solar One and their implications for future central receiver plants, Sol. Energy 47 (1991) 39–47, https://doi.org/10.1016/0038-092X(91)90061-Z.

[66] A. Bonk, S. Sau, N. Uranga, M. Hernaiz, T. Bauer, Advanced heat transfer fluids for direct molten salt line-focusing CSP plants, Prog. Energy Combust. Sci. 67 (2018) 69–87, https://doi.org/10.1016/j.pecs.2018.02.002.

[67] AD2000, AD 2000-Regelwerk: Taschenbuch - Ausgabe 2020, Beuth Verlag GmbH, 2020.

[68] e.V. DDIfN, EN 10028-7 - Flat Products Made of Steels for Pressure Purposes - German Version. Part 7: Stainless Steels, 2016, https://doi.org/10.31030/2398417.

[69] Holdsworth Robertson, ECCC Data Sheets, European Creep Collaborative Committee, 2005.

[70] Bonk A. Thermal energy storage using solar salt at 620 °C: how a reactive gas atmosphere mitigates corrosion of structural materials. SolarPaces 2022. Albuquerque2022.

[71] F. Klasing, T. Hirsch, C. Odenthal, T. Bauer, Techno-economic optimization of molten salt concentrating solar power parabolic trough plants with packed-bed thermocline tanks, Journal of Solar Energy Engineering. 142 (2020), https://doi.org/10.1115/1.4046463.

[72] S. Gage, Technical performance of refractory liners for molten chloride salt thermal energy storage systems, in: SolarPACES 2020: National Renewable Energy lab. (NREL), CO (United States), Golden, 2020 (Medium: ED; Size: 1.5 MB).

[73] S.H. Gage, J.J. Bailey, D.P. Finegan, D.J.L. Brett, P.R. Shearing, C.S. Turchi, Internal insulation and corrosion control of molten chloride thermal energy storage tanks, Sol. Energy Mater. Sol. Cells 225 (2021) 111048, https://doi.org/10.1016/j.solmat.2021.111048.

[74] P. Roos, A. Haselbacher, Thermocline control through multi-tank thermal-energy storage systems, Appl. Energy 281 (2021) 115971, https://doi.org/10.1016/j.apenergy.2020.115971.

[75] J.D. Osorio, R. Hovsapian, J.C. Ordonez, Effect of multi-tank thermal energy storage, recuperator effectiveness, and solar receiver conductance on the performance of a concentrated solar supercritical CO2-based power plant operating under different seasonal conditions, Energy 115 (2016) 353–368, https://doi.org/10.1016/j.energy.2016.08.074.

[76] J.D. Osorio, A. Rivera-Alvarez, M. Swain, J.C. Ordonez, Exergy analysis of discharging multi-tank thermal energy storage systems with constant heat extraction, Appl. Energy 154 (2015) 333–343, https://doi.org/10.1016/j.apenergy.2015.05.018.

[77] A.I.H. Committee, Properties and Selection—Irons, Steels, and High-performance Alloys, ASM International, 1990.

[78] J.B. Ferguson, H. Lopez, K. Cho, C.-S. Kim, Temperature effects on the tensile properties of precipitation-hardened Al-Mg-Cu-Si alloys, Metals 6 (43) (2016), https://doi.org/10.3390/met6030043.